Granular slumping on a horizontal surface

E. Lajeunesse
Laboratoire de Dynamique des Systèmes Géologiques, Groupe de Recherche sur l'Erosion et les Eaux Continentales, Institut de Physique du Globe de Paris, 4 place Jussieu, 75252 Paris Cedex 05, France

J. B. Monnier and G. M. Homsy
Department of Mechanical and Environmental Engineering, University of California, Santa Barbara, California 93106

(Received 16 February 2005; accepted 2 September 2005; published online 7 October 2005)

We report the results of an experimental investigation of the flow induced by the collapse of a column of granular material (glass beads of diameter d) over a horizontal surface. Two different setups are used, namely, a rectangular channel and a semicircular tube, allowing us to compare two-dimensional and axisymmetric flows, with particular focus on the internal flow structure. In both geometries the flow dynamics and the deposit morphologies are observed to depend primarily on the initial aspect ratio of the granular column $a=H_i/L_i$, where H_i is the height of the initial granular column and L_i its length along the flow direction. Two distinct regimes are observed depending on a: an avalanche of the column flanks producing truncated deposits for small a and a column free fall leading to conical deposits for large a. In both geometries the characteristic time scale is the free fall of the granular column $\tau_c=\sqrt{H_i/g}$. The flow initiated by Coulomb-like failure never involves the whole granular heap but remains localized in a surface layer whose size and shape depend on a and vary in both space and time. Except in the vicinity of the pile foot where the flow is pluglike, velocity profiles measured at the side wall are identical to those commonly observed in steady granular surface flows: the velocity varies linearly with depth in the flowing layer and decreases exponentially with depth in the static layer. Moreover, the shear rate is constant, $\dot{\gamma}=0.3\sqrt{g/d}$, independent of the initial aspect ratio, the flow geometry, position along the heap, or time. Despite the rather complex flow dynamics, the scaled deposit height H_f/L_i and runout distance $\Delta L/L_i$ both exhibit simple power laws whose exponents depend on a and on the flow geometry. We show that the physical origin of these power laws can be understood on the basis of a dynamic balance between acceleration, pressure gradient, and friction forces at the foot of the granular pile. Two asymptotic behaviors can be distinguished: the flow is dominated by friction forces at small a and by pressure forces at large a. The effect of the flow geometry is determined primarily by mass conservation and becomes important only for large a. © *2005 American Institute of Physics*. [DOI: 10.1063/1.2087687]

I. INTRODUCTION

The flow of dense granular material is a common phenomenon in engineering applications such as the transport of minerals or cereals and in geophysical situations such as rock avalanches, landslides, and debris or pyroclastic flows. Despite the large number of investigations devoted to this subject, constitutive equations for dense granular flows are still lacking. The approach generally used to circumvent this difficulty has been to derive depth-averaged conservation equations and introduce empirical friction coefficients and velocity profiles deduced from experiments.[1–4] This approach has been successful in describing granular flows in simple situations such as flow along inclines[5,6] and even some geophysical granular flow events.[7,8] However, it presents two important shortcomings. First, depth-averaged equations are valid only if the flowing layer is thin compared to its lateral dimension. Second, the empirical rheological laws are deduced from measurements of quantities (e.g., flow thickness and velocity profiles) performed under steady flow conditions. These cast doubt on the validity of this approach for thick transient flows.

In this context, two groups[9,10] have recently reported experimental studies of the transient flow occurring when a granular mass is suddenly released on a horizontal surface. Both experiments consisted of loading a mass of granular material in a hollow cylinder resting on a horizontal surface. The resulting granular column of initial height H_i and radius L_i was then released "en masse" by quickly removing the cylinder and spread on the horizontal plane until it came to rest, forming a deposit of final height H_f and radius L_f. This experimental situation is particularly attractive because it offers the opportunity to explore the limits of the depth-averaged approach by observing an unsteady thick dense granular flow in a simple geometry.

The difference between Refs. 9 and 10 essentially lies in the kind of granular material and the properties of the spreading surface investigated. Lube *et al.*[9] explored the effect of the density and shape of the grains by using a wide range of granular materials such as salt, sand, and even couscous, sugar, or rice, whereas Lajeunesse *et al.*[10] worked with glass

beads and concentrated on the influence of bead size and substrate properties (rough or smooth, erodible or rigid). Both drew the same striking conclusion: the flow duration, the spreading velocity, the final extent of the deposit, and the fraction of energy dissipated during the flow can be scaled in a quantitative way independent of substrate properties, bead size, density, and shape of the granular material and released mass M. These quantities depend only on the aspect ratio of the initial granular column $a=H_i/L_i$. In particular, the runout $\Delta L=(L_f-L_i)$ follows a simple power law $\Delta L/L_i \propto \sqrt{a}$ at large a.

More recently Balmforth and Kerswell[11] studied the collapse of granular columns in rectangular channels and focused on the deposit shape. As in the axisymmetric case, they observed that the runout is well represented at large a by a simple power-law dependence, whose exponent varies slightly with the channel width $\Delta L/L_i \propto a^{0.65}$ in a narrow channel whereas $\Delta L/L_i \propto a^{0.9}$ in a wide channel. The constants of proportionality of the power laws were found to depend on the granular material internal friction angle.

Three attempts to model granular column collapse within the framework of shallow water equations have been made. Denlinger and Iverson[12] were the first to perform numerical simulations of axisymmetric granular column collapse using depth-averaged equations. Their model, relying on mass and momentum conservation and intergranular stress generation governed by Coulomb friction, was formulated in order to account for the effect of nonzero vertical acceleration on depth-averaged mass and momentum fluxes and stress state. Although their model seems to reproduce the experimental observations, it was not used for a systematic study of the dependence of the runout on the control parameters.

More recently, Kerswell,[13] taking advantage of the similarity between granular slumping and the classical "dam-break" problem in fluid mechanics, solved both the axisymmetric and two-dimensional (2D) granular dam-break problems under the shallow-water approximation. Mangeney *et al.*[14] performed numerical simulations of axisymmetric granular column collapse using depth-averaged equations. Both groups worked under the assumptions of plug flow and effective basal Coulomb friction and did not take into account the effect of vertical acceleration. Although both models exhibit good qualitative agreement with experimental results, they predict that the runout increases linearly with a, significantly overestimating the runout when a becomes larger than unity. Note that the Rankine coefficient is set to unity in the model of Mangeney *et al.*[14] whereas it is a function of the internal and bed friction angles in the model of Kerswell.[13] However, as discussed by Kerswell,[13] differences of Rankine coefficients only affect the constant of proportionality of the power law without modifying the power-law exponents. Finally, when this work was being prepared for publication, we became aware of similar experiments by Siavoshi and Kudrolli.[15] Although they were conducted over the limited range of very small a, they agree with our results in the region of overlap in parameters.

The experimental results of Lube *et al.*,[9] Lajeunesse *et al.*[10] and Balmforth and Kerswell[11] provide strong experimental constraints to test both the limits of the depth-averaged equations and the rheology of granular materials. The slumping of a granular mass remains poorly understood and many questions are still open. Among these are the following: What is the influence of the experimental configuration on runout? What mechanism initiates the flow? What is the thickness of the flowing zone and how does it evolve in time? What are the velocity profiles in the flowing layer? How can complex flow dynamics produce deposits obeying simple power laws? We present in this paper the results of an experimental study aimed at addressing these questions. This is achieved by studying the slumping of a granular mass in two different experimental configurations, allowing us to investigate the internal structure of 2D and axisymmetric spreading flows.

The paper is organized as follows. The two experimental setups and data acquisition are described in Sec. II. The objective of Sec. III is to clarify the influence of the flow geometry. This is achieved by comparing the flow phenomenology (flow duration, runout, final deposit height, etc.) in the rectangular channel to that in the axisymmetric configuration. In Sec. IV we go one step further by investigating the internal flow structure with particular focus given to the flow localization and the velocity profiles within the flowing layer. In Sec. V we propose a physical interpretation of the scalings observed for the runout on the basis of a very simple dynamical balance. The paper ends with a summary of the results and conclusions.

TABLE I. Avalanche, repose, and bed friction angles of the glass beads used for the experiments.

Angle	Glass beads of diameter $d=1.15$ mm	Glass beads of diameter $d=3$ mm
θ_r	$22\pm0.5°$	$22\pm0.5°$
θ_a	$27.4\pm0.5°$	$27.4\pm0.5°$
θ_s	$24.8\pm0.2°$	$14.3\pm0.2°$
θ_w	$11\pm0.3°$	$12.5\pm0.7°$

II. APPARATUS AND PROCEDURE

A. Material properties

We used two different granular materials: glass beads of density $\rho_0=2500\ \mathrm{kg/m^3}$ and of diameter of either $d=1.15$ mm or $d=3$ mm. The repose and avalanche angles of the beads θ_r and θ_a were estimated from the variations of the slope along a granular pile built by slowly pouring beads from a small height. The bed friction angle between the beads and the sandpaper surface, denoted θ_s, and that between the beads and the glass wall, denoted θ_w, were also estimated by determining when a rigid block of particles held together within a paper cylinder would begin to slide on a surface covered with sandpaper or made of glass. Each measurement was repeated several times and the uncertainties were estimated from the dispersion in the data. The results are summarized in Table I.

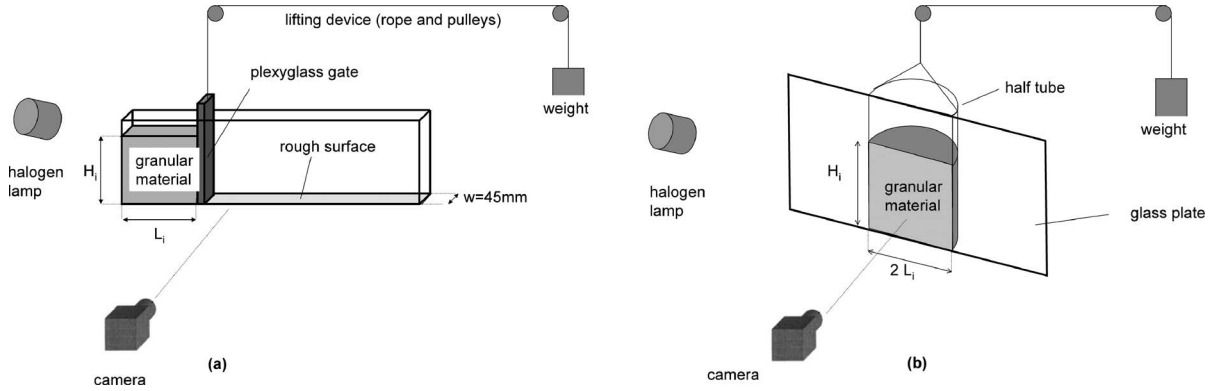

FIG. 1. Schematics of the two experimental configurations investigated: (a) the rectangular channel and (b) the "semiaxisymmetric" setup.

B. Experimental setup and protocol

One experimental configuration is the rectangular channel displayed in Fig. 1(a). It is made of two vertical transparent glass plates of length 100 cm and height 30 cm separated by a uniform spacer ensuring a constant gap thickness $W=45$ mm. The glass plates are thick enough (8 mm) to avoid bending. The horizontal channel base is lined with sandpaper of roughness of the order of 200 μm. The head of the channel is fitted with a vertical Plexiglas gate, creating a reservoir that allows us to suddenly release a large granular mass.

The experimental procedure consists of partially filling the reservoir with a mass M of granular material so as to form a rectangular heap of length L_i, height H_i, and thickness W. The gate is then quickly removed to release the granular mass that spreads in the horizontal channel until it comes to rest. The location of the gate can be moved along the channel, allowing us to vary L_i. In order to ensure reproducible initial conditions, the gate was always opened up in the same way: a weight was dropped and the gate was lifted by a system of ropes and pulleys. We also verified that the time necessary to lift the gate remained small compared to the time necessary to set the granular mass in motion for the whole range of H_i explored.

The other experimental configuration, shown in Fig. 1(b), will be referred to in the rest of the paper as the "semiaxisymmetric" setup. It consists of a Plexiglas half cylinder of inner radius 39 mm held vertically on a horizontal surface covered with the same sandpaper. This is achieved by means of a metal frame which holds the half cylinder against a vertical glass plate of length 60 cm and height 30 cm. The experimental procedure is similar to that used for the rectangular channel. It consists of partially filling the half-cylinder with a mass M of granular material forming a semicircular column. The half-cylinder is then quickly lifted to release the granular mass. To facilitate comparison between experiments performed in the rectangular channel and those performed in the semiaxisymmetric geometry, the initial height and radius of the granular half column will be denoted H_i and L_i.

To ensure reproducible initial conditions, both containers were always filled following the same procedure: the glass beads were poured via a funnel onto a sieve placed above the apparatus, resulting in a homogeneous downfall of grains. The mean packing density of the granular column was estimated by $\phi=M/\rho_0 V_i$, where ρ_0 is the density of the granular material and V_i is the volume of the initial granular heap. ϕ was found to vary slightly between 0.61 and 0.63.

Although no specific antistatic precaution was applied, the beads were large enough to prevent electrostatic effects in the ambient relative humidity of the laboratory, which varied between 60% and 66%. No sign of electrostatic charge transfer such as unusual dust accumulation on the particle and glass walls, or of a humidity effect, such as formation of particles aggregates, was ever observed.

C. Data acquisition

The beads were illuminated via a continuous halogen lamp and the avalanche process was filmed with a 1024 $\times$ 1024 pixel fast camera acquiring 1000 images/s. The camera was carefully aligned along the horizontal direction so as to acquire side views of the granular mass. The spatial resolution achieved in these conditions varied between 0.1 and 0.2 mm/pixel. The camera was interfaced to a computer and the digitized images were processed in order to extract the different quantities of interest.

III. INFLUENCE OF THE GEOMETRY ON THE SLUMPING PHENOMENOLOGY

The experiments performed in the semiaxisymmetric setup are completely consistent with the previous experiments of Lajeunesse *et al.*,[10] who worked with a fully circular tube: the same flow phenomenology illustrated in Fig. 2 is observed for the same range of a, and deposits obtained with the semiaxisymmetric setup follow the same power laws as experiments in the full axisymmetric geometry. In this section we therefore focus on the spreading phenomenology in the rectangular channel and compare it to the semiaxisymmetric case.

A. Flow description

The sequences of images in Fig. 3 illustrate the different flow regimes and deposit morphologies observed in the 2D rectangular channel. The flow phenomenology is very similar to that observed for axisymmetric collapses.[9,10] The flow dynamics depend mainly on the initial aspect ratio a. For small

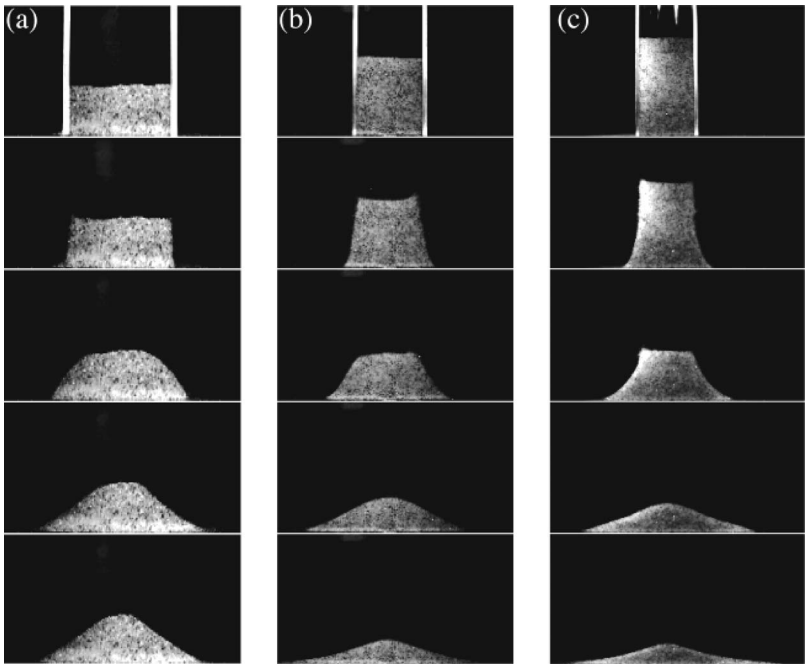

FIG. 2. Three sequences of images corresponding to $d=1.15$ mm beads spreading in the semiaxisymmetric setup. The first image of each sequence corresponds to the moment where the gate is being lifted, the time interval between the following images is $\Delta t=\sqrt{H_i/g}$, except for the last image taken at the very end of the flow when the heap is at rest. (a) Regime 1 $a=0.6$, $M=100$ g, $L_i=39$ mm, $\Delta t=49$ ms. (b) Regime 1 $a=2.4$, $M=400$ g, $L_i=39$ mm, $\Delta t=98$ ms. (c) Regime 2 $a=3.6$, $M=600$ g, $L_i=39$ mm, $\Delta t=120$ ms.

a the granular mass spreads through avalanching of the flanks, producing either truncated cone deposits for $a<0.74$ [Fig. 3(a)] or conical deposits for $a>0.74$ [Fig. 3(b)]. A transition towards a different flow regime is observed when a is increased. This second flow regime is illustrated in Fig. 3(c): upon release, the upper part of the granular mass descends, conserving its shape while the foot of the pile propagates along the channel. Along the deposit an inflection point separates a steep sloped from a large, almost flat region.

Figure 4 shows the time evolution of the profiles of three different granular heaps of the same initial aspect ratio $a=3.2$ but obtained with different masses or bead sizes. The profiles $h(x,t)$ are scaled with respect to L_i and the time interval between two consecutive profiles is scaled with respect to the free-fall time of the granular column $\tau_c=\sqrt{H_i/g}$. The three profiles are identical at each time. This observation demonstrates that, for fixed granular material and substrate properties, the flow dynamics and the final deposit morphology do not depend on the volume of granular material released but only depend on a. The range of substrate and material properties (including the bead size) explored in this paper is too restricted to evaluate their influence. Note however that the observations of Lajeunesse *et al.*[10] and Balmforth and Kerswell[11] indicate that properties such as the bead

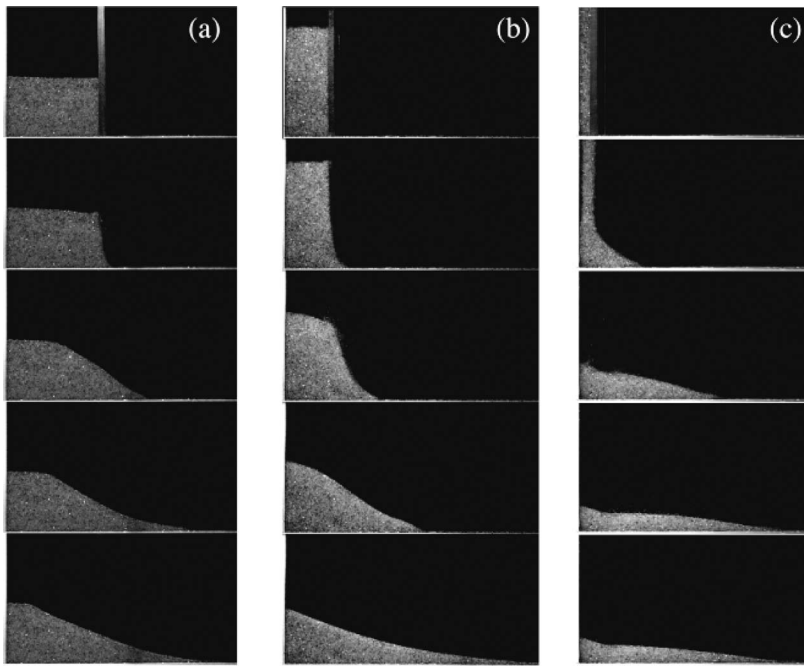

FIG. 3. Same as Fig. 2 but in the rectangular channel. (a) Regime 1, $a=0.6$, $M=470$ g, $L_i=102$ mm, $\Delta t=80$ ms. (b) Regime 1, $a=2.4$, $M=560$ g, $L_i=56$ mm, $\Delta t=117$ ms. (c) Regime 2, $a=16.7$, $M=170$ g, $L_i=10$ mm, $\Delta t=130$ ms.

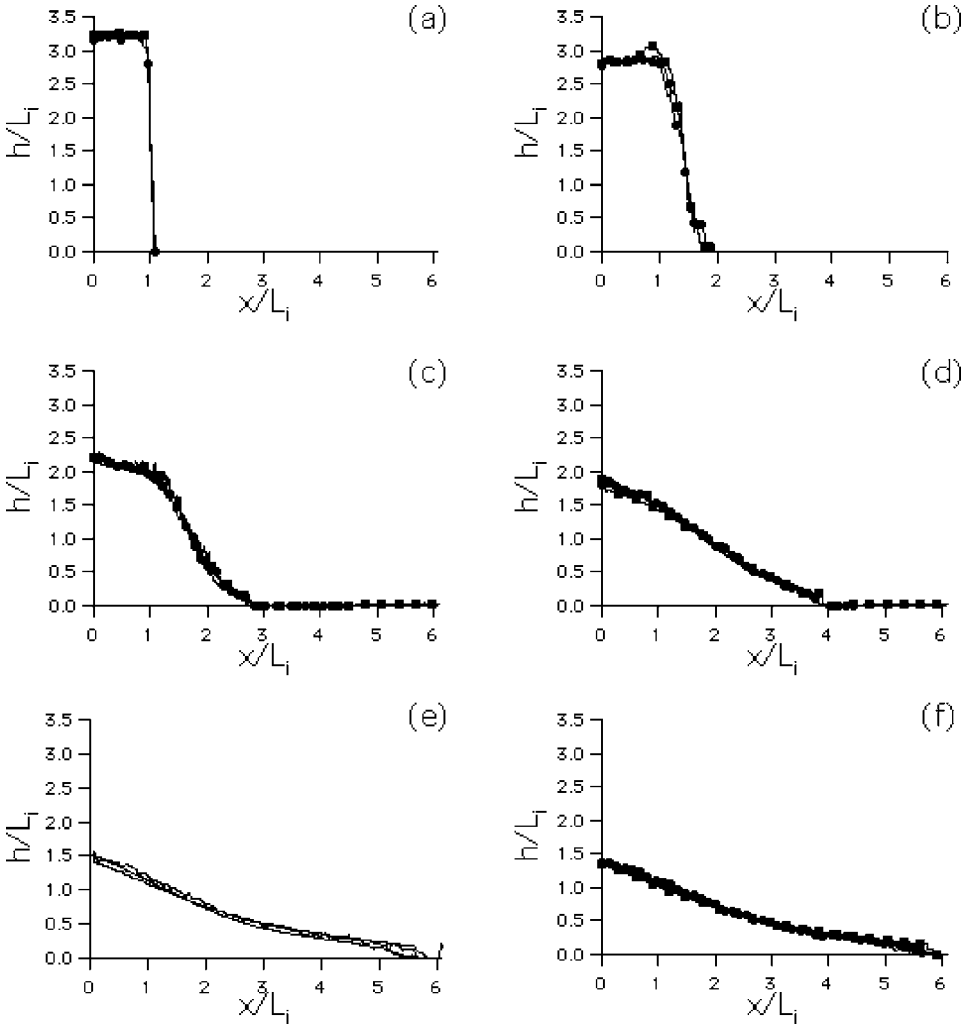

FIG. 4. Sequence of scaled profiles $h(x,t)/L_i$ of three different granular heaps of same initial aspect ratio $a=3.2$ but obtained with different masses or bead sizes. (a) $t=0$, (b) $t=0.5\tau_c$, (c) $t=\tau_c$, (d) $t=2\tau_c$, (e) $t=3\tau_c$, and (f) final deposit. The plain line profiles correspond to $M=650$ g, $L_i=5.3$ cm, and $d=1.15$ mm. The plain line with circles profiles correspond to $M=650$ g, $L_i=5.3$ cm, and $d=3$ mm. The dotted line profiles correspond to $M=162.5$ g, $L_i=2.6$ cm, and $d=1.15$ mm. The different curves are barely distinguishable.

size, the granular material internal friction angle, or the substrate roughness exert an influence on the spreading dynamics.

The results in Fig. 4, together with dimensional analysis, strongly suggest that τ_c is the characteristic time scale in our experiments. To verify this, we compared the flow dynamics for different values of a by tracking the position $L(t)$ of the front (or granular pile foot) in all experimental runs. The results are illustrated in Fig. 5, where we display the normalized distance traveled by the pile foot $(L-L_i)/L_i$ as a function of the scaled time t/τ_c for three different values of a. Interestingly, all runs exhibit the same time evolution regardless of the value of a. After a transient acceleration phase lasting approximately $0.8\tau_c$, the foot of the heap moves at a nearly constant spreading velocity V for about $2\tau_c$. Most of the total distance traveled by the foot of the heap is covered during this time interval. Finally, the flow front decelerates and comes to rest in a time on the order of $0.6\tau_c$. The total duration of the flow is therefore of the order of $3\tau_c$ for all values of a. The same behavior is observed in the semiaxisymmetric setup, which is consistent with the observations of Lube *et al.*,[9] who reported a total flow duration on the order of a few multiples of τ_c for axisymmetric collapses.

B. Deposit morphology

The evolution of the deposit shape with a was quantitatively investigated by measuring the scaled deposit height H_f/L_i and the scaled runout length $\Delta L/L_i=(L_f-L_i)/L_i$, where H_f and L_f are respectively the deposit height and length. The results are plotted in Fig. 6. In order to compare the scaling laws observed in the rectangular channel to these observed in axisymmetric geometries, we have added the data set for axisymmetric collapses from Lajeunesse *et al.*[10] In both geometries and despite rather complex flow dynamics, the scaled deposit height and runout collapse on quite simple power-law curves summarized below:

- In the axisymmetric geometry:

$$\frac{H_f}{L_i}=\begin{cases} a & a\lesssim 0.74, \\ 0.74 & a\gtrsim 0.74, \end{cases}$$

$$\frac{\Delta L}{L_i}\propto\begin{cases} a & a\lesssim 3, \\ a^{1/2} & a\gtrsim 3. \end{cases}$$

- In the rectangular channel:

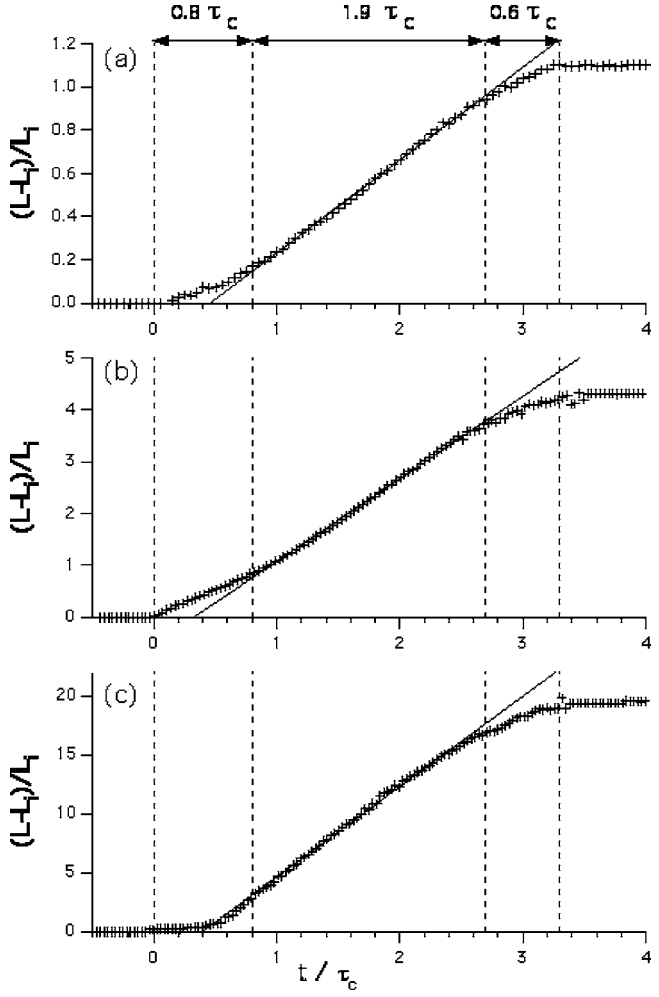

FIG. 5. Scaled distance traveled by the pile foot $[L(t)-L_i]/L_i$ as a function of t/τ_c. (a) $a=0.6$, $M=470$ g, $L_i=102$ mm. (b) $a=2.4$, $M=560$ g, $L_i=56$ mm. (c) $a=16.7$, $M=170$ g, $L_i=10$ mm.

$$\frac{H_f}{L_i} \propto \begin{cases} a & a \lesssim 0.7, \\ a^{1/3} & a \gtrsim 0.7, \end{cases}$$

$$\frac{\Delta L}{L_i} \propto \begin{cases} a & a \lesssim 3, \\ a^{2/3} & a \gtrsim 3. \end{cases}$$

Note that the power-law exponent of the runout observed in our rectangular channel is identical to the one reported by Balmforth and Kerswell[11] for a narrow channel.

Let us first comment on the behavior of the runout displayed in Fig. 6(a). Two different regimes are observed depending on the range of a. For small a, namely $a \lesssim 3$, $\Delta L/L_i$ increases linearly with a for both flow geometries. In other words, the runout ΔL increases linearly with H_i, a result that is easily obtained from dimensional analysis.[9] It is also for this range of a that shallow-water equations show good agreement with the experimental data.[13,14]

For $a \gtrsim 3$, the scaled runout does not vary linearly with a but follows a power law whose exponent depends on the flow geometry as summarized above. Two different mechanisms are likely to account for this crossover. First, vertical acceleration, which is negligible at low a, becomes important when a increases. Second, pressure gradients, which scale as $\rho_0 g a$, are likely to be small compared to friction forces at small a but become important at large a. The change of power-law exponents observed for $a \approx 3$ might therefore be interpreted as the transition between small a flows dominated by friction and large a flows where vertical acceleration and pressure gradient effects become predominant. Note also that the mass conservation expressions are different in the rectangular and the axisymmetric geometries, which may account for the different power-law exponents for large a.

The deposit height exhibits two different regimes characterized by changes of power-law exponents depending on the range of a [see Fig. 6(b)]. For $a \lesssim 0.7$, all the data fall on the same line independent of the flow geometry: $H_f/L_i \approx a$. This is of course a trivial consequence of the fact that $H_f = H_i$ for the truncated cone deposits observed in this range of a.

For $a \gtrsim 0.7$, two different behaviors are observed depending on the flow geometry. In the axisymmetric geometry, the scaled deposit height roughly saturates at a value of the order of 0.74.[10] In the rectangular channel, it increases as $a^{1/3}$. Interestingly this latter result is recovered in two recent 2D numerical investigations of the collapse of a granular column of disks using contact dynamics.[16,17] The similarity between the experiments and the numerical simulations (performed without a wall) strongly suggests that the differences between the evolution of H_f/L_i in the axisymmetric geometry and that in the rectangular channel are not an experimental artifact due to the friction at the wall of the rectangular channel but have their origin in the geometry itself.

No model has yet provided a fully satisfactory explanation of the slumping dynamics that has revealed the physical origin of the different power-law exponents reported above. This is what motivates the investigation of the internal flow structure reported in the next section.

IV. INTERNAL FLOW STRUCTURE

We used two different tools in order to probe the internal structure of the slumping granular mass. First, the shape and evolution of the flowing layer were investigated by calculating the intensity difference between two consecutive images. The result is then thresholded so as to distinguish between static regions, which appear as black pixels, and the flowing layer, where the motion of the beads appears as white pixels. In practice, one needs to evaluate the noise caused by lighting fluctuations or intrinsic vibrations of camera and apparatus. The intensity difference between two consecutive images of the pile at rest shows that lighting fluctuations are negligible compared to the signal generated by the flowing beads, provided the time interval between the two images is larger than about $\Delta t=5$ ms. We chose to work with $\Delta t=10$ ms, which turned out to be long enough to achieve a good signal-to-noise ratio, and small enough compared to the characteristic slumping time scale τ_c. Typical sequences of image differences observed for different initial aspect ratios a in both flow geometries are displayed in Figs. 7 and 8.

We also measured the velocity field in the flowing layer using a particle image velocimetry (PIV) algorithm based on

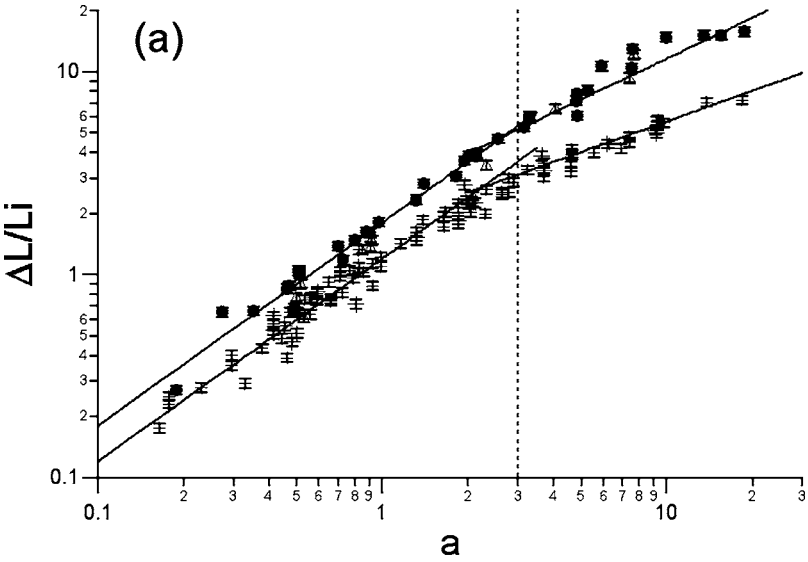

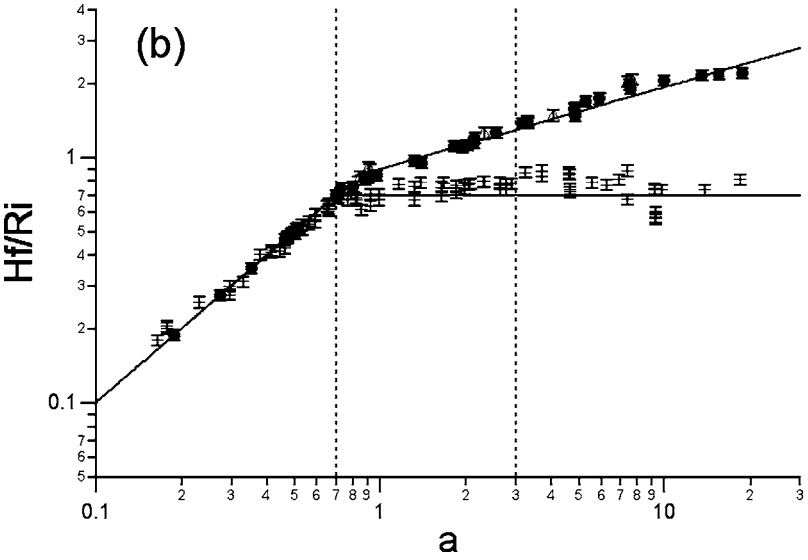

FIG. 6. Scaled runout $\Delta L/L_i$ (a) and scaled deposit height H_f/L_i (b) as functions of a. Circles and triangles correspond to experiments performed in the 2D channel working respectively with glass beads of diameter $d=1.15$ mm or $d=3$ mm. Crosses correspond to the data set of axisymmetric collapses from Lajeunesse *et al.* (Ref. 10).

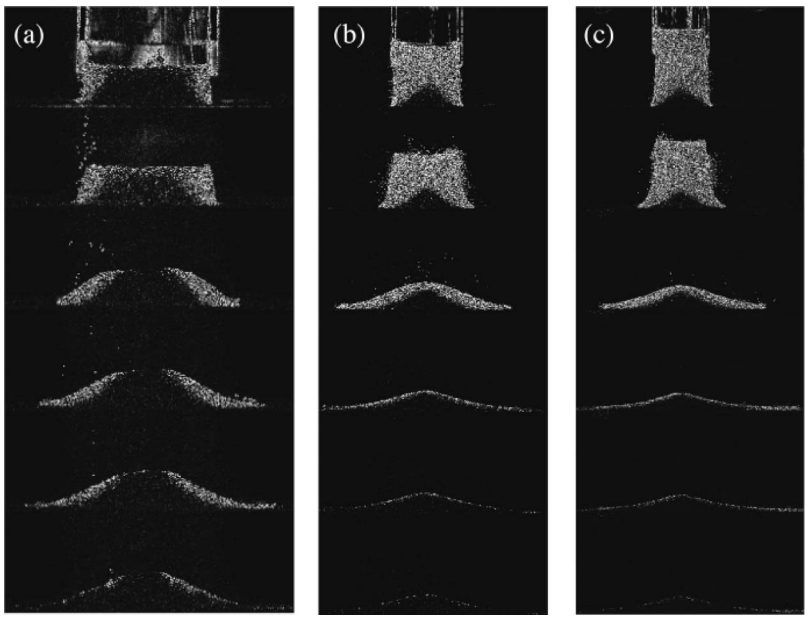

FIG. 7. Sequence of successive image differences corresponding to experiments performed in the semiaxisymmetric setup. (a) $a=0.6$, $L_i=39$ mm, $M=100$ g, and $d=1.15$ mm: $t=0.5\tau_c$, τ_c, $2\tau_c$, $3\tau_c$, $4\tau_c$, and $6\tau_c$. (b) $a=2.4$, $L_i=39$ mm, $M=400$ g, and $d=1.15$ mm: $t=0.5\tau_c$, τ_c, $2\tau_c$, $3\tau_c$, $3.5\tau_c$, and $4\tau_c$. (c) $a=3.6$, $L_i=39$ mm, $M=600$ g, and $d=1.15$ mm: $t=0.5\tau_c$, τ_c, $2\tau_c$, $3\tau_c$, $3.5\tau_c$, and $4\tau_c$.

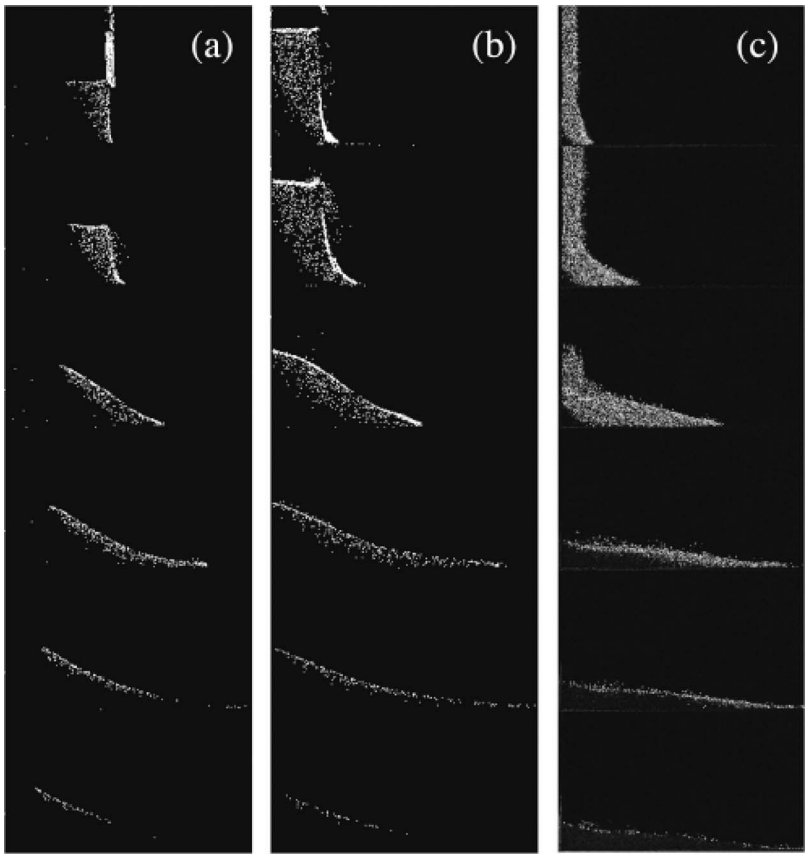

FIG. 8. Sequence of successive image differences corresponding to experiments performed in the rectangular channel. (a) $a=0.6$, $M=470$ g, $L_i=102$ mm, and $d=1.15$ mm: $t=0.5\tau_c$, τ_c, $2\tau_c$, $3\tau_c$, $5\tau_c$, and $7\tau_c$. (b) $a=2.4$, $M=560$ g, $L_i=56$ mm, and $d=1.15$ mm: $t=0.5\tau_c$, τ_c, $2\tau_c$, $3\tau_c$, $4\tau_c$, and $5\tau_c$. (c) $a=16.7$, $M=170$ g, $L_i=10$ mm, and $d=1.15$ mm: $t=0.5\tau_c$, τ_c, $2\tau_c$, $3\tau_c$, $3.5\tau_c$, and $4\tau_c$.

the correlation between two consecutive images of small boxes within the flow. The size of the correlation box was 32×32 pixels, corresponding to 4×4 bead diameters, and the time interval between two consecutive images was 2 ms, achieving an accuracy of the order of 3 mm/s. Typical vertical velocity profiles measured at the side wall are shown in Figs. 9 and 10. Although measured in the rectangular channel, these velocity profiles are similar to those measured in the semiaxisymmetric geometry as discussed in the following.

These velocity profiles are measured at the wall, and hence one might ask to what extent they are relevant to what is going on inside the granular mass far from the wall. This difficult question was partially addressed by observing the slumping from above so as to measure the surface velocity field. In the rectangular channel, we observed small sidewall effects as illustrated in Fig. 10(c): the surface velocity profile between the two sidewalls is that of a plug flow with a high slip velocity at the wall and low shear along the direction transverse to the flow. Systematic measurements indicated that the ratio of the maximum surface velocity to the surface velocity at the wall remained between 1.2 and 1.4. In the semiaxisymmetric case, we never observed any modification of the surface velocity field near the wall: the surface velocity remained perfectly radial and there was no significant change of velocity at the wall. In the following we will therefore consider that vertical velocity profiles at the wall provide a good estimate of the vertical velocity profiles in the bulk far from the wall.

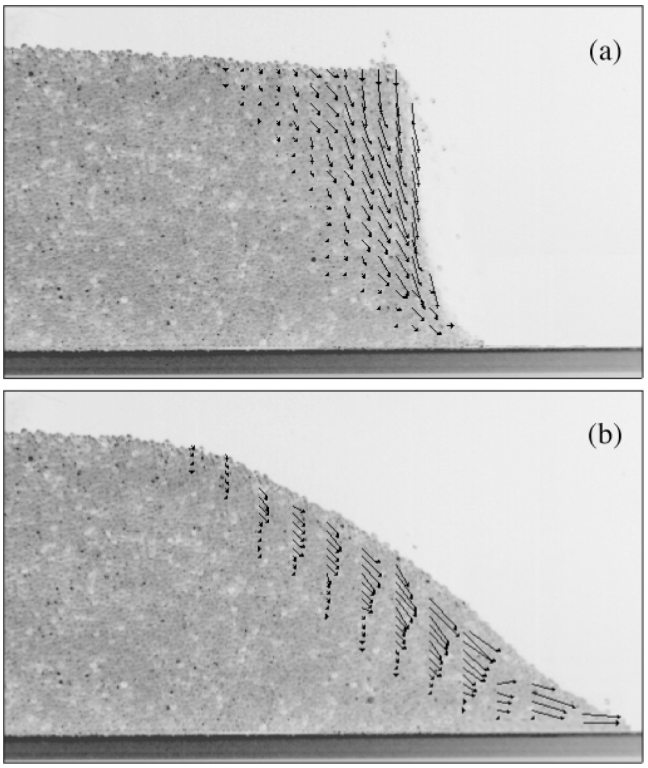

FIG. 9. Velocity field at the wall of the rectangular channel, $a=0.46$, $L_i=10.8$ cm, $M=400$ g, and $d=1.15$ mm. (a) $t=30$ ms$=0.4\tau_c$ and (b) $t=92$ ms$=1.3\tau_c$.

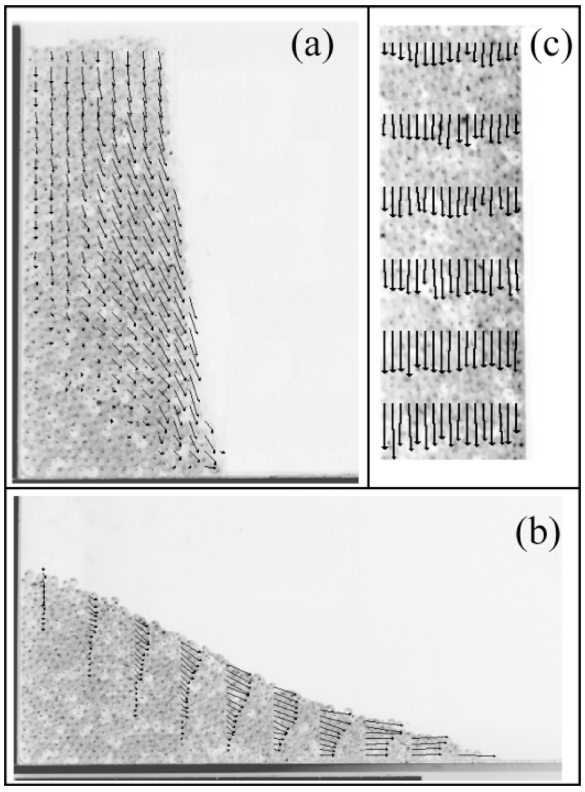

FIG. 10. Velocity fields observed at the wall of the rectangular channel for $a=3.2$. $L_i=5.3$ cm, $M=650$ g, and $d=3$ mm. (a) $t=40$ ms$=0.3\tau_c$ and (b) $t=229$ ms$=1.7\tau_c$. (c) Velocity field at the pile surface between the walls at $t=229$ ms$=1.7\tau_c$.

A. Evolution of the internal flow structure with the initial aspect ratio *a*

Using image difference and PIV measurements, we observed two distinct behaviors depending on the value of the initial aspect ratio a, independent of the flow geometry. At small a ($a \lesssim 0.7$) the flow is initiated by failure at the edge of the pile along a well-defined fracture surface above which material slides down and below which grains remain static [see Figs. 7(a) and 8(a)]. Figure 9(a) shows a snapshot of a velocity field typical of the very beginning of the flow: the grains located above the fracture move "en masse" and those located below remain static so that most of the shear is located along the fracture.

After a transient of the order of τ_c, the flow is fully developed. The velocity field then depends on the position along the pile [see Fig. 9(b)]. In the vicinity of the front, flow involves the whole pile thickness and the corresponding velocity profile is that of a plug flow in the horizontal direction. Far from the front, flow is localized in an upper layer beneath the free surface and the velocity profiles, locally parallel to the static/flowing interface, is composed of an upper linear part in the flowing layer and a lower exponential tail in the static granular bed. Note that this velocity profile is similar to those commonly measured in steady granular surface flows.[4] As the pile spreads, the rim separating the distal flowing and the proximal motionless region propagates progressively inward, an effect that is more pronounced in the rectangular channel. For initial aspect ratios $a \lesssim 0.7$, the flow stops before the central motionless plateau is totally consumed, leaving a "truncated-cone-like" deposit of final height $H_f=H_i$.

For larger a ($a \gtrsim 0.7$), the flow is still initiated by failure along a well-defined surface (an inclined plane in the 2D geometry or a cone in the axisymmetric one) as illustrated in Figs. 7(b), 7(c), 8(b), and 8(c). However, in that case the initial granular column is much higher than the top of the failure surface. Due to gravity, most of the granular column falls along the vertical direction, as is visible from the velocity field shown in Fig. 10(a). Note that when they reach the vicinity of the summit of the failure surface, the grains are deviated toward the horizontal direction, thus probably dissipating a lot of the kinetic energy acquired during free fall. During a transient of the order of the free-fall time τ_c, the initial granular column completely collapses and progressively evolves towards either a conical pile in the axisymmetric geometry, or a triangular one in the rectangular channel, along which a surface flow develops. At this stage the velocity field is identical to the one observed for small a [see Fig. 10(b)]: horizontal plug flow near the pile foot and a linear velocity profile connected to an exponential tail in the rest of the heap.

For $a \gtrsim 0.7$, the resulting deposit is a cone. Interestingly its height H_f coincides with the summit of the failure surface in the axisymmetric geometry. This explains the plateau $H_f/H_i=0.74$ observed at large a in the axisymmetric geometry shown in Fig. 6(b). This is very different than what happens in the rectangular channel, where the deposit summit always lies above the top of the failure surface.

As pointed out before, the comparison between recent numerical investigations of the collapse of a 2D granular column using contact dynamics[16,17] and our experimental data demonstrates that the difference between the evolution of H_f in the axisymmetric geometry and its evolution in the rectangular channel is not an experimental artifact due to the sidewall friction but is probably a geometrical effect.

Regardless of the experimental configuration and for all values of a, the flow is initiated by rupture along a well-defined surface above which material slides down and below which grains remain static. Systematic measurements show that the failure angle remains of the order of 50°–55° regardless of a or of the experimental configuration. This value is consistent with an interpretation in terms of active Coulomb failure, which leads to a predicted failure angle $\theta_y=45°+\delta/2$, where δ is the internal friction angle of the granular material. Estimating δ from the repose angle leads to $\theta_y=45°+22°/2=56°$, in relatively good agreement with the experimental observations. Note that, contrary to the suggestion of Lajeunesse *et al.*,[10] this fracture angle does not account in a straightforward way for the transition between truncated cone and conical deposit occurring at $a \sim 0.7$.

Finally let us note that although the spreading of the granular mass ceases after a time $t \sim 3\tau_c$, some motion persists along the free surface for much longer times as shown by the last images of Figs. 7 and 8. These motions, located behind the foot, are due to internal rearrangement and secondary avalanches, the duration of which can last up to $t \sim 6\tau_c$.

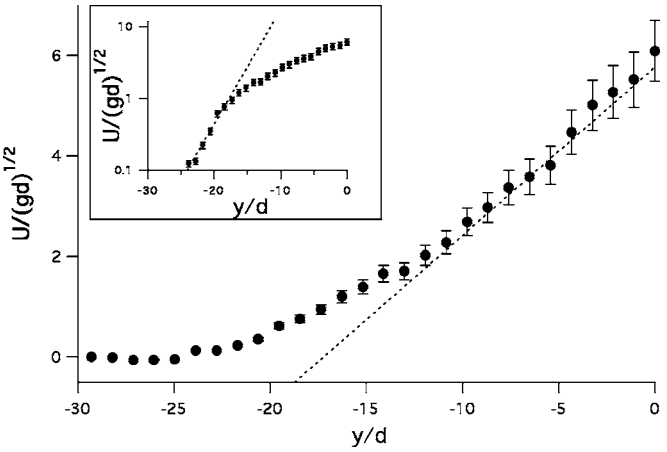

FIG. 11. Typical normalized velocity profile $u/\sqrt{gd}$ at the wall of the rectangular channel as a function of normalized depth y/d measured along the transverse flow direction ($a=0.51$, $t=4.2\tau_c$, $d=1.15$ mm). The y origin coincides with the free surface of the heap. The dotted line corresponds to a linear fit of the profile in the flowing layer. Inset: Same velocity profile in a linear-log plot demonstrating the exponential tail. The dotted line corresponds to an exponential fit of the data in the static bed.

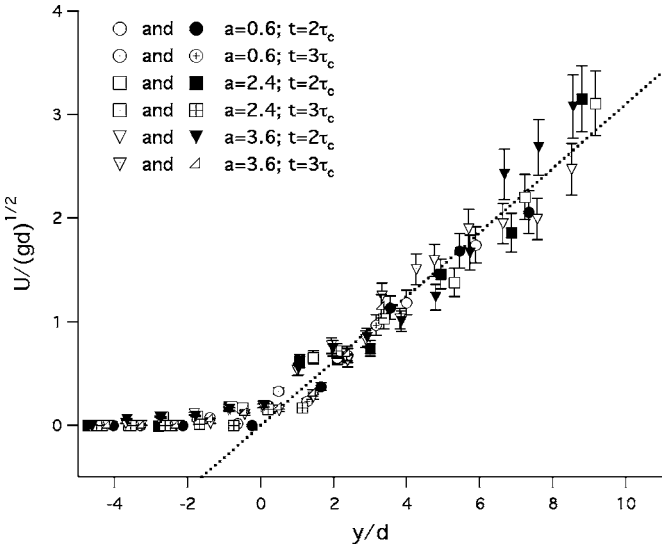

FIG. 12. Normalized velocity profiles $u/\sqrt{gd}$ at the wall of the semiaxisymmetric setup as a function of the normalized depth y/d. The profiles have been translated along the y axis to make their static/flowing interface coincide at the y origin. The different symbols correspond to different initial aspect ratio a, different times and different positions along the heap as indicated on the figure.

B. Internal velocity profiles

In this subsection, we focus on the shape of the fully established velocity profiles observed when $t > \tau_c$. As pointed out in the previous section, the flow is locally parallel to the static/flowing interface. The velocity profiles are therefore measured in their natural frame of reference, i.e., along the direction locally transverse to the flow. Figure 11 shows a typical velocity profile in the rectangular channel. The same behavior is observed in the semiaxisymmetric geometry. The velocity varies linearly with depth in the flowing layer and decreases exponentially with depth in the static layer (see the inset of Fig. 11). As pointed out in Sec. IV A, such a velocity profile is very close to those in steady granular surface flows.[4]

To put this observation on more quantitative ground we performed several experiments varying the initial aspect ratio a and the bead size d in both the rectangular channel and the semiaxisymmetric setup. For each run we measured several velocity profiles at regular time intervals and at equally spaced positions along the heap. Figure 12 displays some of these velocity profiles measured in the semiaxisymmetric geometry. Velocity is normalized by $\sqrt{gd}$ and depth y by d. All profiles have been translated along the y axis to make their static/flowing interface coincide at the y origin: the linear parts of the velocity profiles collapse rather well onto the same line.

We performed the same analysis on the velocity profiles measured in the rectangular channel. The normalized velocity profiles are compared to those observed in the semiaxisymmetric geometry in Fig. 13: the linear part of all the velocity profiles collapse rather well along the same line of slope 0.3. In other words, the shear rate in the flowing layer is constant, $\dot{\gamma}=0.3\sqrt{g/d}$, and independent of the initial aspect ratio and of the flow geometry.

To summarize, the unsteady surface flow exhibits the same velocity profile (upper linear part in the flowing layer and a lower exponential tail in the static granular bed) as steady flows, and the shear rate in the flowing layer scales as $\dot{\gamma} \propto \sqrt{g/d}$ in both cases.

This latter result apparently contradicts work by Courrech du Pont *et al.*[18] These authors measured velocity profiles during transient dry granular avalanches and found that it follows a pure exponential decrease with no well-developed linear part. However, the maximum shear rate reached during their avalanches was smaller than the constant shear rate value observed in the linear profiles,

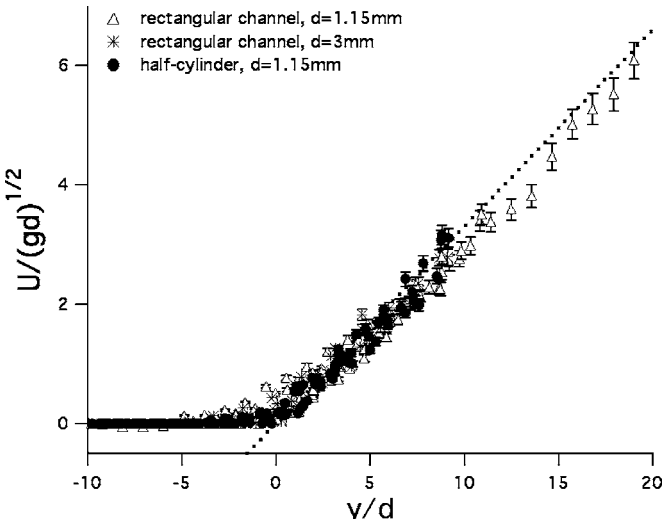

FIG. 13. Normalized velocity profiles at the wall for various initial aspect ratios a, bead sizes d, different times, and different positions along the heap. Circles, triangles, and stars correspond to measurements performed in the semiaxisymmetric geometry with $d=1.15$ mm, the rectangular channel with $d=1.15$ mm, and the rectangular channel with $d=3$ mm, respectively. The profiles have been translated along the y axis to make their static/flowing interface coincide at the y origin.

$O(\sqrt{g/d})$. As pointed out by the authors,[18] the fact that this critical shear rate is not reached might explain why they do not observe linear velocity profiles. On the other hand, the shear rate exceeds this critical value in our experiments, thus accounting for the development of a linear part in our velocity profiles.

A last remark concerns the effects of sidewalls. Jop *et al.*[19] have recently investigated steady uniform granular surface flows in rectangular channels. They measured the mass flow rate at the channel outlet, the velocity profiles at the wall, and the thickness of the flowing layer in the bulk far from the wall using a weakly intrusive method. They demonstrated that the properties (velocity profile and flowing layer thickness) of steady uniform granular surface flows are completely controlled by the presence of sidewalls and proposed a theoretical model accounting for their observations. It is therefore surprising that we recover the same velocity profiles both in the rectangular channel where the flows takes place between two sidewalls and in the semiaxisymmetric geometry where it takes place along a single wall.

V. MODEL

A. Comments on the shallow-water approximation

To summarize the experimental observations, the flow can be schematically divided into two stages:

Stage 1: Fall of the granular column leading to the formation of a pile, either conical in the axisymmetric geometry or triangular in the rectangular channel. During this transient, which lasts for about τ_c (stage 1), vertical acceleration is important at large a.

Stage 2: Spreading of the granular pile until it comes to rest after a time interval of the order of $2.5\tau_c$. During this second stage, the flow does not involve the whole heap but remains localized in a layer below the free surface, whose shape varies in time and depends on a.

These observations highlight the difficulties in modeling the collapse of a granular column within the frame of shallow-water assumptions. A comprehensive model should account for vertical momentum transfer associated with the downfall of the column (stage 1) and describe the surface flow forming during the second stage of the flow. However, the equations solved by Kerswell[13] and Mangeney *et al.*[14] do not account for any of these mechanisms as they are derived under the assumption of negligible vertical momentum transfer, plug flow, and basal friction. As a result, shallow water models cannot reproduce the exact shape of the spreading granular mass, especially at large a, where momentum transfer associated to the vertical downfall of the granular column is important.

Note that, surprisingly, shallow-water models capture some of the experimental behavior (in particular the runout) at low aspect ratios[11,13,14] even though the contrast between surface flows and static underlayer is important for this range of a (see Fig. 8). This suggests that the plug flow assumption is not critical to capture the runout behavior, especially if the basal friction coefficient is used as a fitting parameter. Our feeling is that the main challenge is to account for vertical momentum transfer. This probably explains the failure of shallow-water models to predict the experimental values of runout at large a, and also explains why they capture the experimental behavior at low aspect ratios where vertical momentum transfer is small.

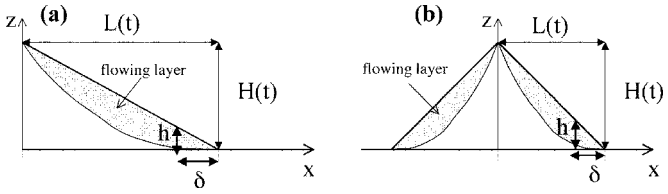

FIG. 14. Schematic view of the spreading granular mass after the transient collapse of the initial column. The pile is triangular in the rectangular channel (a) and conical in the axisymmetric geometry (b). In both cases the flowing layer is localized at the free surface except in the vicinity of the pile foot where a plug velocity profile spans the whole depth.

To summarize, a comprehensive model of the collapse of a granular column should account for vertical momentum transfer associated with the fall of the column (stage 1) and describe the surface flow that is established during the second stage of the flow. To our knowledge, such a model is not yet available. Possible alternatives might be to use a modified shallow-water model accounting for the effect of nonzero vertical acceleration such as the one proposed by Denlinger and Iverson[12] or one of the set of equations[20,21] proposed to describe granular surface flows that take into account the presence of an erodible static/flowing interface.

Complete modeling of the collapse of a granular column is beyond the scope of the present paper. Instead, we will now take advantage of the experimental observations to propose a simple model that can describe the scaling of runout distance as a function of a.

B. Simplified model

The experimental observations show that the granular pile does not spread much during the fall of the column (stage 1). In fact, 85%–90% of the total runout distance is achieved during the second stage of the flow, which lasts for about $2.5\tau_c$ and during which the granular mass has a conical or triangular shape (see Fig. 5). This suggests focusing on stage 2. We now take advantage of this experimental observation to develop a simple model.

Let us first consider a granular mass spreading in a rectangular channel and write a conservation of horizontal momentum on an elementary slice of material of width W, length δ, and thickness h located at the pile foot, as sketched in Fig. 14(a). In the vicinity of the foot, a plug velocity profile spans the whole thickness. As a result, momentum conservation in this region reduces to a force balance between the friction force at the bed level and a force F_x related to the normal stress exerted along the left side of the slice:

$$\frac{d(mU)}{dt} = (F_x - \mu mg), \tag{1}$$

where U is the velocity of the pile foot, $m = 1/2\rho_0 Wh\delta$ is the mass of the elementary slice, and μ is the coefficient of friction between the layer and the bed.

Assuming that the pressure is hydrostatic and given by $\rho_0 gz$, and assuming that the horizontal and vertical normal stresses are proportional, one gets

$$F_x = W\int_0^h K\rho_0 gz\,dz = W\frac{K}{2}\rho_0 gh^2, \tag{2}$$

where K is the Rankine (or earth-pressure) coefficient.

The velocity profile is pluglike at the pile foot and hence the mass m of the elementary slice is conserved. As a result, Eqs. (1) and (2) lead to

$$\frac{dU}{dt} = \frac{d^2L}{dt^2} = g\left(K\frac{h}{\delta} - \mu\right), \tag{3}$$

where $L(t)$ is the instantaneous position of the pile foot. Using the same argument, one recovers the same result in the axisymmetric geometry.

Note that Eq. (3) is valid only in the vicinity of the pile foot where the flowing layer involves the whole heap thickness. Far from the pile foot, we are dealing with a surface flow and Eq. (3) should be modified in order to account for the possible exchanges of mass and momentum between static and flowing layers.

The next step is to assume that, during the second stage of the flow, the slope is constant along the whole pile. This strong assumption is roughly justified by images of Figs. 2 and 3, and its validity will be discussed in more detail in the following. This assumption leads to $h/\delta = H(t)/L(t)$ so that one obtains

$$\frac{d^2L}{dt^2} = g\left(K\frac{H(t)}{L(t)} - \mu\right), \tag{4}$$

where $H(t)$ is the instantaneous height of the pile. Note that Eq. (4) is not correct in the case of truncated cones observed for $a < 0.7$. However, as discussed later, the pressure gradient tends to be negligible for this range of a so that we do not need to discuss its form for the case $a < 0.7$.

To go one step further, we need to express $H(t)$ as a function of $L(t)$. This is achieved through overall mass conservation, which reads

$$H(t)\,.\,L(t)^n = \alpha H_i L_i^n, \tag{5}$$

where α and n depend on the flow geometry: $\alpha=2$ and $n=1$ in the rectangular channel whereas $\alpha=3$ and $n=2$ in the axisymmetric geometry.

Combining Eqs. (4) and (5) finally leads to

$$\frac{d^2L}{dt^2} = g\left(\alpha K\frac{H_i L_i^n}{L^{n+1}} - \mu\right), \tag{6}$$

which describes in an approximate way the propagation of the foot of the conical or triangular pile.

A formal solution of Eq. (6) is not relevant as it does not describe the initial stages of the collapse, so we ignore the initial conditions. Instead we will just use dimensional analysis to check if such a simplified force balance is likely to capture the experimental scalings. In particular, note that the pressure term $\alpha K H_i L_i^n / L^{n+1}$ is of order a so that two different asymptotic behavior can be distinguished depending on the value of a.

1. Small initial aspect ratios ($a \ll \mu$)

For $a \ll \mu$, Eq. (6) simplifies to

$$\frac{d^2L}{dt^2} = -g\mu. \tag{7}$$

Equation (7) implies on dimensional grounds that the runout distance should scale as

$$\Delta L \propto g\mu\tau_c^2, \tag{8}$$

where τ_c is the characteristic flow time scale (known to be controlled by the free fall of the initial column) $\tau_c = \sqrt{H_i/g}$, so that one obtains

$$\frac{\Delta L}{L_i} \propto \mu a, \tag{9}$$

in agreement with the experimental scalings measured for $a \lesssim 3$ both in the rectangular channel and in the axisymmetric geometry (see Fig. 6).

2. Large initial aspect ratios ($a \gg \mu$)

For $a \gg \mu$, Eq. (6) simplifies to

$$\frac{d^2L}{dt^2} = g\alpha K\frac{H_i L_i^n}{L^{n+1}}. \tag{10}$$

Similarly, Eq. (10) implies on dimensional grounds that the runout should scale as

$$\Delta L \propto gK\tau_c^2\frac{H_i L_i^n}{\Delta L^{n+1}}, \tag{11}$$

which finally leads to

$$\frac{\Delta L}{L_i} \propto a^{2/n+2} \propto \begin{cases} a^{2/3} & \text{in the rectangular channel,} \\ a^{1/2} & \text{in the axisymmetric geometry,} \end{cases} \tag{12}$$

again in agreement with the experimental measurements (see Fig. 6). Note also that Eq. (10) implies that changing K only affects the constant of proportionality of the power law but does not change its exponent, in agreement with the observations of Balmforth and Kerswell.[11]

C. Discussion

The model proposed here nicely reproduces the phenomenology observed experimentally. However, a key assumption is that of a constant slope along the whole pile during the second stage of the flow. If this assumption is correct, we see from Eq. (5) that the following relationship should be verified:

$$\frac{H(t)}{L(t)} = \alpha\frac{H_i L_i^n}{L(t)^{n+1}}. \tag{13}$$

$H(t)/L(t)$ was compared to $\alpha H_i L_i^n / L(t)^{n+1}$ for several experimental runs performed in both geometries and for initial aspect ratios up to 6.0. We were not able to measure $H(t)/L(t)$ for $a > 6.0$ because the top of the pile remained out of the field of view during most of the experiment. In all cases, we observed that Eq. (13) held approximately as soon as t

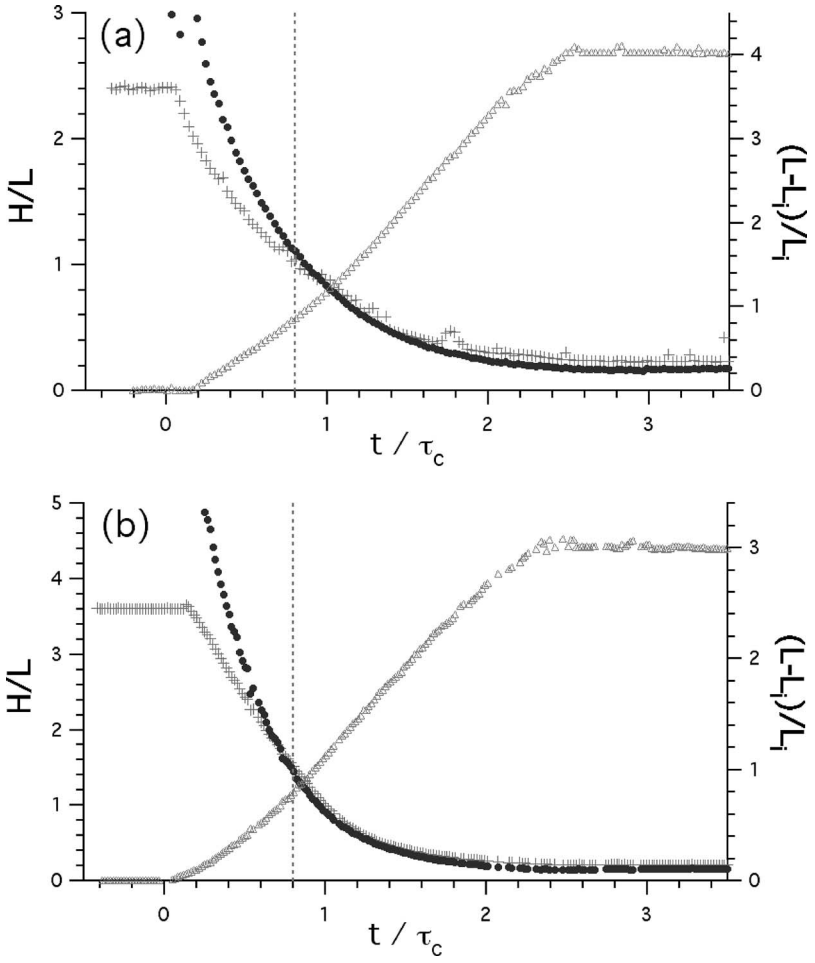

FIG. 15. (a) $H(t)/L(t)$ (crosses), $H_iL_i/L(t)^2$ (circles), and $[L(t)-L_i]/L_i$ (triangles) as a function of t/τ_c. Data obtained in the rectangular channel with $a=2.4$, $L_i=56$ mm, $d=1.15$ mm, and $M=560$ g. (b) $H(t)/L(t)$ (crosses), $3H_iL_i^2/L(t)^3$ (circles), and $[L(t)-L_i]/L_i$ (triangles) as a function of t/τ_c. Data obtained in the semiaxisymmetric setup with $a=3.6$, $L_i=39$ mm, $d=1.15$ mm, and $M=600$ g.

$\gtrsim 0.8\tau_c$, that is, when entering the second stage of the flow (see Fig. 15). This result confirms the assumption of a constant slope along the whole pile.

To summarize, this simple model allows us to understand the physical origin of the power laws measured for the runout in terms of a simple balance between pressure gradient and friction forces. Two asymptotic behaviors can be distinguished: the flows is dominated by friction at small a and by the pressure gradient at large a. The effect of the flow geometry is encoded in the conservation of mass and becomes important only at large initial aspects ratios a.

Although this simple model does not describe the initial stage during which the column collapses, it reproduces fairly well the experimental scalings. This might lead us to think that the initial transient during which the granular column collapses plays a negligible part in the process determining the runout. This is not true, however. On the contrary, this transient plays a key role in selecting the runout through the determination of the flow time scale τ_c, which was used as an empirical fact in the model.

VI. SUMMARY AND CONCLUSIONS

We have reported an experimental study of the slumping of a granular mass over a horizontal surface in a rectangular channel and in a semiaxisymmetric geometry. Our objectives were as follows: first, to clarify the influence of the flow geometry on the flow and on the runout and, second, to investigate the flow structure, with particular focus on the flow localization and the velocity profiles. This was achieved by using two different experimental setups designed to investigate the internal flow structure, namely a rectangular channel and a semicircular tube apparatus.

The main results are as follows:

- The flow phenomenology is qualitatively very similar in the rectangular channel and in the axisymmetric geometry. In both cases we recover the same flow dynamics and deposit morphologies as a function of the initial aspect ratio a: an avalanche of the column flanks producing truncated deposits at low a and a column free fall leading to conical deposits at larger a.
- Upon release the flow is initiated by Coulomb-like failure along a well-defined surface, above which material slides down "en masse" and below which grains remain static so that most of the shear is located along the fracture. This observation is consistent with the results of Balmforth and Kerswell,[11] who reported a slight dependency on the constants of proportionality of the above power laws with the granular material internal friction angle.
- The characteristic time scale of the flow following the initial failure is controlled by the free fall of the granular column: $\tau_c=\sqrt{H_i/g}$. This flow can be schematically divided into the following stages: collapse of the column leading to

the formation of a pile, either conical in the axisymmetric geometry or triangular in the rectangular channel, during a transient of the order of τ_c (stage 1), and spreading of this pile until it comes to a rest for about $2.5\tau_c$ (stage 2).
- The flow never involves the whole granular heap but remains localized in a surface layer, whose shape and size depends on a and which varies in time.
- Except in the vicinity of the pile foot where the flow is pluglike, velocity profiles measured at the wall are identical to those commonly observed in steady granular surface flows:[4] the velocity varies linearly with depth in the flowing layer and decreases exponentially with depth in the static layer. Once the flow is fully developed ($t > \tau_c$), the linear parts of the velocity profiles collapse along the same line independent of the initial aspect ratio, the flow geometry, position along the heap, or time, demonstrating that the shear rate is constant, $\dot{\gamma}=0.3\sqrt{g/d}$. This surprising result suggests that for large enough shear rates unsteady granular surface flows exhibit the same velocity profiles as the steady ones.
- In both experimental configurations, the scaled deposit height and runout obey simple power laws summarized below:

  In the axisymmetric geometry:

$$\frac{H_f}{L_i} = \begin{cases} a & a \lesssim 0.74, \\ 0.74 & a \gtrsim 0.74, \end{cases}$$

$$\frac{\Delta L}{L_i} \propto \begin{cases} a & a \lesssim 3, \\ a^{1/2} & a \gtrsim 3. \end{cases}$$

  In the rectangular channel:

$$\frac{H_f}{L_i} \propto \begin{cases} a & a \lesssim 0.7, \\ a^{1/3} & a \gtrsim 0.7, \end{cases}$$

$$\frac{\Delta L}{L_i} \propto \begin{cases} a & a \lesssim 3, \\ a^{2/3} & a \gtrsim 3. \end{cases}$$

- Although the dynamics involved is very complex, the physical origin of the power laws measured for the runout can be understood on the basis of a dynamic balance between acceleration, pressure gradient, and friction forces at the foot of the pile. Two asymptotic behaviors can be distinguished: low initial aspect ratio flows dominated by friction forces and large initial aspect ratio flows dominated by pressure gradients. The effect of the flow geometry is determined primarily by mass conservation and becomes important only at large values of a.

Of course, this simple model is far from describing the whole slumping process and there are still many open questions. In particular, it is very important to achieve a clear understanding of the mechanisms governing the free fall of the granular column and the conversion of vertical to horizontal momentum as these processes appear to control the flow time scale τ_c and therefore the final runout distance. Recent numerical investigations using contact dynamics[16,17] that allow evaluation of quantities not accessible experimentally are likely to provide important new insights on this aspect. Modified shallow-water models accounting for the effect of vertical momentum transfer[12] might also prove useful.

A last important point concerns the effect of sidewall in the rectangular channel. Balmforth and Kerswell[11] reported a slight dependence of the exponent of the runout power law with channel width. Although not taking into account sidewall effects, our simple dynamical balance predicts the correct scalings for the narrow channel case, i.e., precisely where sidewall effects are expected to play an important part. A recent experimental investigation of steady granular surface flows in rectangular channels[19] has shown that surface velocity profiles (i.e., those viewed from above) are less and less uniform in the transverse direction when the channel is enlarged. Assuming that this result holds for unsteady flows, it would mean that the flow is no longer 2D in a wide channel, thus accounting for the modification of the power laws reported by Balmforth and Kerswell.[11] In other words, the choice would be between a 2D flow with strong sidewall effect or a 3D flow with weaker sidewall effects. This explanation is however rather speculative and the effect of sidewalls remains an open problem.

ACKNOWLEDGMENTS

We thank G. Bienfait, Y. Gamblin, and A. Viera for their invaluable technical assistance in designing and realizing the experimental setup. We are indebted to C. D. Meinhart for his help in developing our PIV measurements. We also thank B. Andreotti, J. Hinch, H. Huppert, C. Jaupart, R. Kerswell, F. Metivier, O. Pouliquen, L. Staron and all the members of the GDR Midi for many fruitful discussions. The authors acknowledge partial support of this work by the U.S. Department of Energy, Office of Basic Energy Sciences.

[1] S. B. Savage and K. Hutter, "The motion of a finite mass of granular material down a rough incline," J. Fluid Mech. **199**, 177 (1989).
[2] O. Pouliquen, "Scaling laws in granular flows down rough inclined planes," Phys. Fluids **11**, 542 (1999).
[3] R. M. Iverson and J. W. Vallance, "New views on granular mass flows," Geology **29**, 115 (2001).
[4] G. D. R. Midi, "On dense granular flows," Eur. Phys. J. E **14**, 341 (2004).
[5] K. Hutter, T. Koch, C. Pluss, and S. B. Savage, "The dynamic of avalanches of granular materials from initiation to runout. Part. II experiments," Acta Mech. **109**, 127 (1995).
[6] O. Pouliquen and Y. Forterre, "Friction law for dense granular flows: application to the motion of a mass down a rough inclined plane," J. Fluid Mech. **453**, 131 (2002).
[7] A. Mangeney, Ph. Heinrich, R. Roche, G. Boudon, and J. L. Cheminée, "Modeling of debris avalanche and generated water waves: Application to real and potential events in Montserrat," Phys. Chem. Earth **25**, 741 (2000).
[8] E. B. Pitman, C. C. Nichita, A. Patra, A. Bauer, M. Sheridan, and M. Bursik, "Computing granular avalanches and landslides," Phys. Fluids **15**, 3638 (2003).
[9] G. Lube, H. Huppert, S. Sparks, and M. Hallworth, "Axisymmetric collapse of granular columns," J. Fluid Mech. **508**, 175 (2004).
[10] E. Lajeunesse, A. Mangeney-Castelnau, and J. P. Vilotte, "Spreading of a granular mass on a horizontal plane," Phys. Fluids **16**, 2371 (2004).
[11] N. J. Balmforth and R. R. Kerswell, "Granular collapse in two dimensions," J. Fluid Mech. **538**, 399 (2005).
[12] R. P. Denlinger and R. Iverson, "Granular avalanches across irregular three-dimensional terrain: 1. Theory and computation," J. Geophys. Res. **109**, F01014 (2004).
[13] R. R. Kerswell, "Dam break with Coulomb friction: A model for granular slumping?" Phys. Fluids **17**, 057101 (2005).

[14] A. Mangeney-Castelnau, F. Bouchut, J. P. Vilotte, E. Lajeunesse, A. Aubertin, and M. Pirulli, "On the use of Saint-Venant equations for simulating the spreading of a granular mass," J. Geophys. Res. **110**, B09103 (2005).
[15] S. Siavoshi and A. Kudrolli, "Failure of a granular step," Phys. Rev. E **71**, 051302 (2005).
[16] R. Zenit, "Computer simulations of the collapse of granular columns," Phys. Fluids **17**, 031703 (2005).
[17] L. Staron and J. Hinch, "Study of the collapse of granular columns using DEM numerical simulation," J. Fluid Mech. (in press).
[18] S. Courrech du Pont, R. Fischer, P. Gondret, B. Perrin, and M. Rabaud, "Instantaneous velocity profiles during granular avalanches," Phys. Rev. Lett. **94**, 048003 (2005).
[19] P. Jop, Y. Forterre, and O. Pouliquen, "Crucial role of side walls for granular surface flows: Consequence for the granular rheology," J. Fluid Mech. (in press).
[20] S. Douady, B. Andreotti, and A. Daerr, "On granular surface flow equations," Eur. Phys. J. B **11**, 131 (1999).
[21] D. V. Khakhar, A. V. Orpe, P. Andresen, and J. M. Ottino, "Surface flow of granular materials: Model and experiments in heap formation," J. Fluid Mech. **441**, 255 (2001).